Computational model of the effect of light scattering from cataracts in the human eye

Ismael Kelly-Pérez,[1,*] Neil C. Bruce,[2] Luis R. Berriel-Valdos,[3] Annette Werner,[1] and José A. Delgado Atencio[4]

[1]*Institute for Ophthalmic Research, Eberhardt-Karls-Universität Tübingen, D-72076 Tübingen, Germany*
[2]*Centro de Ciencias Aplicadas y Desarrollo Tecnológico, Universidad Nacional Autónoma de México, México, D.F. 04510, Mexico*
[3]*Instituto Nacional de Astrofísica, Óptica y Electrónica, Apartado Postal 51 y 216, Tonantzintla, Puebla, C.P. 72000, Mexico*
[4]*Universidad Politécnica de Tulancingo, C.P. 43629, Tulancingo, Hidalgo, Mexico*
**Corresponding author: ismael.kelly-perez@uni-tuebingen.de*

Received April 5, 2013; revised September 19, 2013; accepted October 29, 2013;
posted October 29, 2013 (Doc. ID 188387); published November 21, 2013

A model of the human eye has been developed, including scattering from cataracts inside the nucleus of the lens. The cataracts are modeled as spherical particles with refractive index different from that of the surrounding lens medium. Scattering from the retina is also included in the simulations. Variations of scattering particle diameter, number of particles, and wavelength of the illuminating light are investigated. It is shown that particle size is the most important parameter affecting the scattered light, and that the scattering from the retina can mask the effect of the scattering particles, for some range of the parameters.

OCIS codes: (330.7326) Visual optics, modeling; (330.4060) Vision modeling; (290.2558) Forward scattering; (290.4020) Mie theory.
http://dx.doi.org/10.1364/JOSAA.30.002585

1. INTRODUCTION

Cataracts are one of the most common defects of the human eye [1,2]. They are known to have various causes: prolonged exposure to ultraviolet radiation, secondary effects caused by diseases such as diabetes or hypertension, injuries in the eye, or aging effects [3] (it is estimated that 7 out of every 10 people over the age of 65 will have some form of cataract). The effects of cataracts on the image-forming process in the eye are reduction in contrast sensitivity [4,5] and an increase in the glare and halos produced by bright objects [6,7].

Cataracts are nonuniformities in the lens of the eye that cause opacity or loss of transparency. There are a limited number of ways in which the opacification may occur. According to the location of opacity, cataracts can be classified as subcapsular, nuclear, and cortical, in each of those regions different kinds of microscopic scatterers could be developed [8]. This paper focuses on specific particles that appear in human age-related nuclear cataracts.

Nuclear cataracts are thought to be caused by particles in the lens that have a variation of density, and so of refractive index, from the surrounding medium [9]. Oxidation of parts of the fibers forming the eye lens structure can take place, particularly with advanced age [10]. These damaged parts of the lens can group together to form particles with high molecular weight to cause variations of refractive index [11]. These variations cause scattering of the light passing through the eye, meaning the point spread function (PSF) on the retina deteriorates and the image is not focused correctly. Doctors examine the eye by looking at the light that enters the eye, is scattered from the retina, and then passes through the optical system again to emerge through the iris and the cornea. This light passes through the eye system twice and also includes scattering from the retina. In this work, we propose a model for the scattering caused by cataracts in the human eye, to investigate the relationship between scattering of light in the forward direction, which affects the image reaching the retina, and scattering in the backward direction, which leaves the eye and is used as a diagnostic factor by doctors. We have to mention that particles that produce the opacities inside the lens have a size distribution as has been shown by van den Berg and Spekreijse [8]. In this work, the results we show were obtained by simulating that particles are distributed only inside the nucleus of the lens and all of them have the same size in each simulation process; this is a simplification of the actual problem. We selected four different cases of particle size in order to study how increase in the size of scatterers affects the retinal and pupil image.

2. COMPUTATIONAL MODEL

The model of the human eye used has been constructed using parameters published in the literature [12]. Table 1 shows the data for the parameters used in the model. We have used a model with eight aspheric surfaces and variable refractive index.

The computational model involves a random (Monte Carlo) selection of the positions of rays in the pupil of the eye within a circle of diameter 0.1 mm. All the rays are sent into the eye parallel to the eye's optical axis. The rays are then traced through the aspheric system to find the positions of the rays reaching the retina. The rays are then traced back from the

Table 1. Parameters of the Optical Model of the Human Eye

Surface Number	Radius of Curvature (mm)	Asphericity Q	Refractive Index n	Separation
1	7.83	−0.23	1.333	6
2	7.46	−0.36	1.401	50 μm
3	7.09	−0.46	1.378	500 μm
4	6.718	−0.56	1.357	5 μm
5	6.34	−0.66	1.336	3 mm
6	11.0	−1.0	1.42	3.6 mm
7	−8.0	−0.5	1.336	16 mm
8	−12.0	0		

retina through the system to the pupil of the eye to find the distribution of rays leaving the eye. The rays traced back would be the rays used by doctors for their diagnosis.

The raytracing of light through the aspheric surfaces of the eye model is performed using the equations given by Welford [13]. Here, we present only the most important equations of the method.

To trace rays in the system, the position and direction of the rays must be followed between the surfaces of the system. The first step in tracing a ray through a surface is to calculate the position at which the ray intersects the plane tangent to the vertex of the surface, i.e., tangent to the surface at the optical axis. If a ray has initial position x_i, y_i, z_i and initial direction L_i, M_i, N_i, d_r is the distance moved from the initial position to the tangential plane intersection point, and x'_{i+1}, y'_{i+1}, z'_{i+1} is the position of the tangent plane intersection point, then

$$x'_{i+1} = x + L_i \frac{d_r}{N_i} \tag{1}$$

$$y'_{i+1} = y + M_i \frac{d_r}{N_i} \tag{2}$$

$$z'_{i+1} = \sum_{j=0}^{i} d_j, \tag{3}$$

where $\sum_{j=0}^{i} d_j$ is the total distance moved by the ray from the coordinate origin. Next, the distance from the tangent plane intersection point to the intersection point on the surface, along the ray, is found. Denoting this distance as Δ, it can be shown that

$$\Delta = \frac{F}{G + [G^2 - cF(1 + QN^2)]^{\frac{1}{2}}}, \tag{4}$$

where

$$F = c({x'_{i+1}}^2 + {y'_{i+1}}^2) \tag{5}$$

$$G = N - c(L_i x_{i+1} + M_i y_{i+1}), \tag{6}$$

where c is the paraxial curvature of the surface and Q is the asphericity. Then the position on the surface is given by

$$x_{i+1} = x'_{i+1} + L_i \Delta \tag{7}$$

$$y_{i+1} = y'_{i+1} + M_i \Delta \tag{8}$$

$$z_{i+1} = z'_{i+1} + N_i \Delta. \tag{9}$$

Then, the refraction of the ray has to be calculated to find the new direction of the ray after the surface. It can be shown, using vectorial Snells law, that

$$n_{i+1} L_{i+1} - n_i L_i = k\alpha \tag{10}$$

$$n_{i+1} M_{i+1} - n_i M_i = k\beta \tag{11}$$

$$n_{i+1} N_{i+1} - n_i N_i = k\gamma, \tag{12}$$

where n_i and n_{i+1} are the refractive indices before and after the surface, respectively:

$$k = n_{i+1} \cos I_{i+1} - n_i \cos I_i, \tag{13}$$

with I_i and I_{i+1} the incidence and the refracted angle, respectively, and α, β, and γ the components of the normal vector to the surface at the intersection point.

Scattering of the light inside the eye is considered as having only two sources: the particles distributed in the lens and scattering from the retina. The scattering particles inside the lens are approximated as homogeneous spherical particles of a given size and refractive index [3,11,14]. The sizes of the particles used are 1, 2, 3, and 4 μm. In the literature, the typical size of the cataract particles is around 3 μm [9]. We consider that the refractive indices of the eye lens material and the cataract particles are $n_{\text{lens}} = 1.42$ and $n_{\text{cat}} = 1.49$, respectively. The case studied here is that of nuclear cataracts where the scattering particles are concentrated in the nucleus of the eye lens. To model this case, the central part of the lens (radii of curvature 11.0 and −8.0 mm, separation between surfaces 3.60 mm) is filled with a given number of particles using Strauss process [15–17] to give a random distribution of particles with a minimum particle–particle separation of 10 μm [3], which is typical for cataracts. The number of particles inside the nucleus of the lens was taken to be 100,000, 200,000, 300,000, or 400,000. The raytracing inside the nucleus of the lens involves checking the position of the rays to find those that are intersected by a particle. The intersected rays are scattered by using Mie theory to calculate the angular distribution of scattered intensity, or the phase function, produced by the particle for a given wavelength [18–21]. The normalized phase function is given by

$$P(\theta) = \frac{4\pi}{k^2 \sigma_{\text{sca}}} \frac{(S_1(\theta)^2 + S_2(\theta)^2)}{2}, \tag{14}$$

where the scattering amplitudes are

$$S_1(\theta) = \sum_{n=1}^{\infty} \frac{2n+1}{n(n+1)} [a_n \pi_n(\cos\theta) + b_n \tau_n(\cos\theta)] \tag{15}$$

$$S_2(\theta) = \sum_{n=1}^{\infty} \frac{2n+1}{n(n+1)} [b_n \pi_n(\cos\theta) + a_n \tau_n(\cos\theta)] \tag{16}$$

and n is the mode number, $\pi_n(\cos\theta)$ and $\tau_n(\cos\theta)$ are functions of the Legendre polinomials, and

$$a_n = \frac{m\psi'_n(y)\psi_n(x) - m_{sp}\psi_n(y)\psi'_n(x)}{m\psi'_n(y)\zeta_n(x) - m_{sp}\psi_n(y)\zeta'_n(x)} \tag{17}$$

$$b_n = \frac{m_{sp}\psi'_n(y)\psi_n(x) - m\psi_n(y)\psi'_n(x)}{m_{sp}\psi'_n(y)\zeta_n(x) - m\psi_n(y)\zeta'_n(x)}, \tag{18}$$

where m and m_{sp} are the refractive indices of the material and the particles, respectively, and the Ricatti–Bessel functions are given by

$$\psi_n(z) = zj_n(z) = \sqrt{\frac{\pi}{2z}}J_{n+\frac{1}{2}}(z) \tag{19}$$

$$\chi_n(z) = -zy_n(z) = \sqrt{\frac{\pi}{2z}}Y_{n+\frac{1}{2}}(z) \tag{20}$$

$$\zeta_n(z) = zh_n^{(2)}(z) = \psi_n(z) + i\chi_n(z). \tag{21}$$

The transverse scattering cross section is given by

$$\sigma_{sca} = \frac{2\pi a^2}{x^2}\sum_{n=1}^{\infty}(2n+1)(|a_n|^2 + |b_n|^2) \tag{22}$$

and $x = mka$, where a is the particle size.

The scattered intensity distribution, given by Eq. (14), is used as a probability density distribution for the scattered ray direction. This ray is then propagated until it intersects another particle, in which case it is scattered again, or leaves the lens nucleus, in which case it is traced through the rest of the system.

The scattering of light in the retina was modeled with the method of Marcos and Burns [22,23]. In this method, the light intensity distribution in the pupil of the eye of the light scattered back from the retina is given by

$$I = 10^{\frac{-r^2}{\rho}}, \tag{23}$$

where r is the radial position in the pupil plane and ρ is a measure of the width of the scattered light spot. Following the work of Marcos and Burns [23], the value of $\rho = 9.09$ mm^2 (note that here we are using the inverse of the value given in [22]). Using a simple model of a perfect lens, with a point source at the focal length (which in our model is the distance between the lens and the retina, 16 mm; see Table 1), this means that the 1/10 width of the distribution of scatter angles for the scattering process on the retina is given by

$$\Delta\theta = \tan^{-1}\sqrt{9.09}/16 = 0.186 \text{ rad} \tag{24}$$

so that the function describing the angular distribution of the scattering from the retina is

$$I = 10^{\frac{-\theta^2}{\Delta\theta^2}}, \tag{25}$$

where θ is the scattering angle.

In our model, the rays are traced through the eye system, checking if there is intersection of the ray with scattering particles in the lens. Then, scattered or not, the ray is traced to the retina and the position of the ray on the retina is recorded. The ray is then scattered from the retina, traced back through the system, with scattering from the particles in the lens calculated a second time, until it reaches the pupil plane, and the positions of intersection are recorded again.

3. RESULTS

With our computational model, we aim to show the effect of scattering on the image on the retina and on the light coming back out of the pupil of the eye, and to study the behavior of the scattered light distribution while varying the density of the scattering bodies distributed in the lens and the wavelength of the light. When we run the simulation, we get two matrices that represent the light distribution in the retina and pupil planes. Figure 1 shows the results of the scattering effect upon varying the diameter of the scattering particles while keeping their number, wavelength, and relative refractive index constant. The diameter of the scattering particles varies from 1 to 4 μm. As the density of the particles increases in the lens, it can be observed that in the plane of the retina there is more light away from the central point of the image and, therefore, there is more scattering, resulting in a wider PSF with increasing diameter of the scattering particles. Although it is known that particles with smaller diameter scatter light at larger angles than particles with large diameter [18,19], the fact that the percentage of volume they represent within the lens is smaller means that these particles do not scatter much energy, and, practically, the image point shows very little effect of scattering, as can be seen in the case for the simulation using scattering particles of 1 μm. The number of scattering particles is 400,000 for each of the four (fourth) cases shown. When the size of the spheres is 1 μm, the total volume occupied by the particles is 0.00021 mm^3 and the percentage of volume occupied by these particles within the region where they are distributed is 0.000467%, whereas the volume of 400,000 particles with 4 μm diameter is 0.0134 mm^3 and represents a percentage of 0.0298%. Inside 1 mm^3 of the inner lens, there are an average of 8880 particles. The effect of the density increment when the diameter of the scattering particles increases can be seen clearly in the images formed by the first pass. In this case, the intensity increases outside the central point as we increase the size of the particles. However, in the images formed in the pupil after the photons have been reflected, i.e., after the second pass, the effect of scattering due to the particles is not present. We can notice that the size of the spot in the pupil image seems very similar in every simulation even though the size of the particles has been changed. The scattering efficiency for particles of 1 μm with relative refractive index 1.49/1.42 and illuminated with light of 400 nm wavelength is 0.5802. For particles under the same conditions and with diameters of 2, 3, and 4 μm, the efficiencies are 1.9204, 3.0528, and 3.2781, respectively. As can be seen, while the size of the particle increases, the scattering efficiency is higher. Furthermore, since scattering is in phase in the forward direction regardless of the wavelength, it is expected that scattering in this direction increases with size faster than in any other direction [24]. A general result is, the larger the particle, the greater the scattering in the forward direction, with the effect that the scattering angle range is narrower. Therefore, as the particles become bigger, more light is scattered at lower

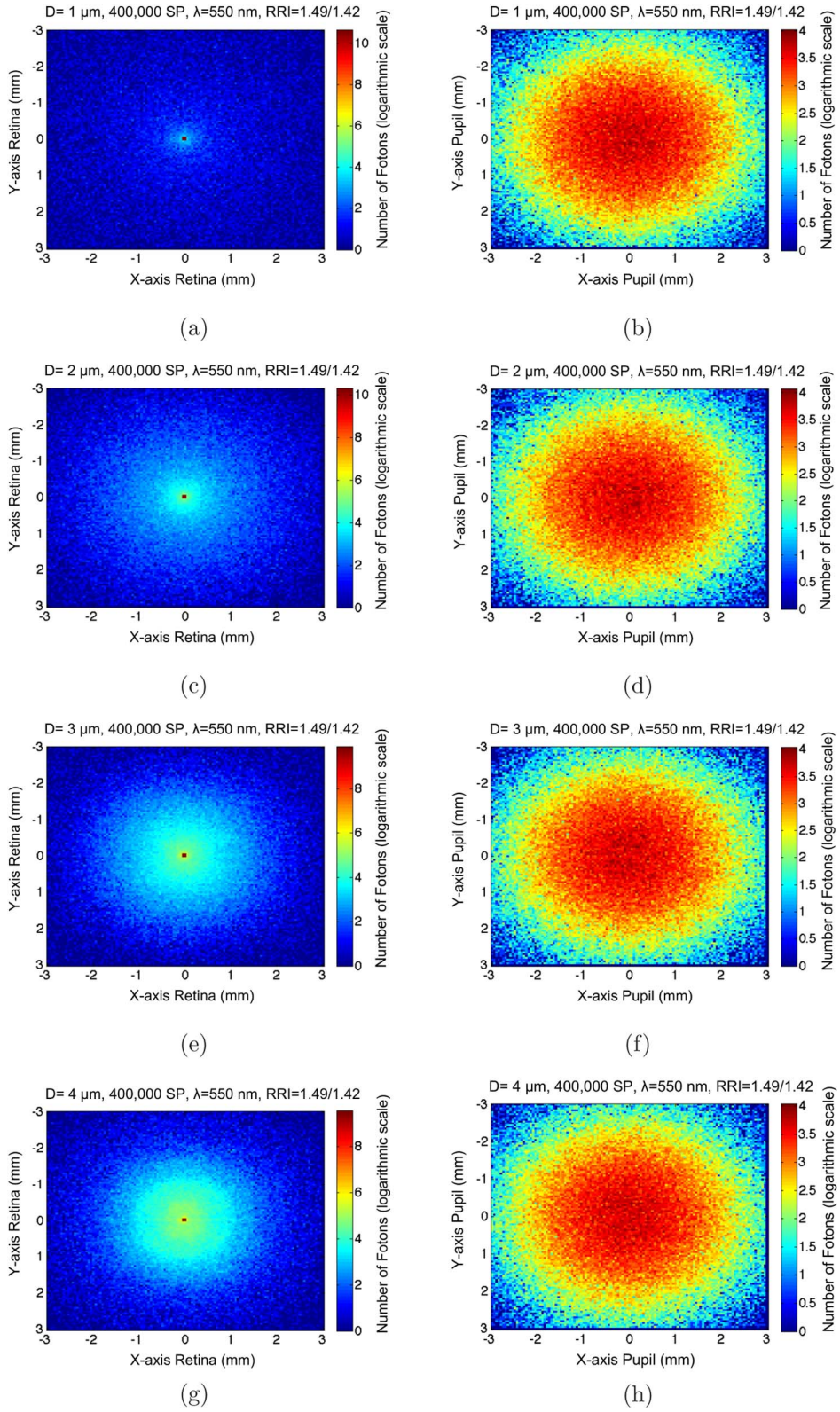

Fig. 1. Comparison of light intensity distribution between retina and pupil planes when size particle is varying. SP, scattering particles.

angles. According to our simulations, the density increase of the inhomogeneities inside the lens, since the size of scatters is bigger, has a very strong effect on the amount of light scattered, as can be seen in the images in the retinal plane that are shown in Fig. 1, where the spot is wider as the density of inhomogeneities increases. Looking at the images that are produced in the second pass, this effect has disappeared and the PSF is very similar among the four cases; even if we compare the images of the PSF in the pupil plane for particles of 1 and 4 μm, the variation in the redistribution of the light due to the scattering cannot be detected. In the first pass, the scattering occurs due to the particles inside the lens,

whereas in the second pass scattering occurs in two media: the retina and the lens.

Figure 2 shows an analysis of the effect of wavelength on the scattered light. For this case, particle size was 3 μm, the number of particles in the lens was 400,000, and relative refractive index was 1.49/1.42. The wavelength values selected in each simulation were 400, 550, and 700 nm, respectively. From Mie solution to Maxwell's equations (Mie scattering), scattering efficiency decreases with increasing wavelength [18,19,24]. When $\lambda = 400$ nm, scattering efficiency is 3.0528; with $\lambda = 550$ nm the value is 2.1702 and with $\lambda = 700$ nm we have 1.5148. On the other hand, as wavelength increases, the range of scattering angles increases slightly, according to the scattering phase functions, which are not shown here. Considering both effects, we can establish that wavelengths close to blue give rise to more scattering in the central region in comparison with wavelengths close to green and red, and this effect is present in a relatively narrower zone surrounding the central point. The images of the PSF for the first pass show that as we increase the wavelength, the size of the center of the spot is reduced and there is more light scattering away from the central image point. The three images formed in the pupil plane show a very similar intensity distribution, indicating that wavelength is not a significant factor in the second pass.

Figure 3 shows a set of images representing the PSF obtained with our model when we increased the number of scattering particles in the lens. For these cases, particle size was 4 μm, wavelength was 550 nm, and the index of refraction ratio was 1.49/1.42. Results are shown for 100,000, 200,000, 300,000, and 400,000 scattering particles. As the number of particles increases, changes can be seen in the intensity distributions in the borders of the images 1 to 2.5 mm from the center of the image. According to our model, in this zone it is possible to identify changes in the number of scattering particles inside the lens due to the increase in intensity distribution in this area. The images for the pupil plane do not show the same effect, as we can notice that the light intensity distributions in this spot are all very similar.

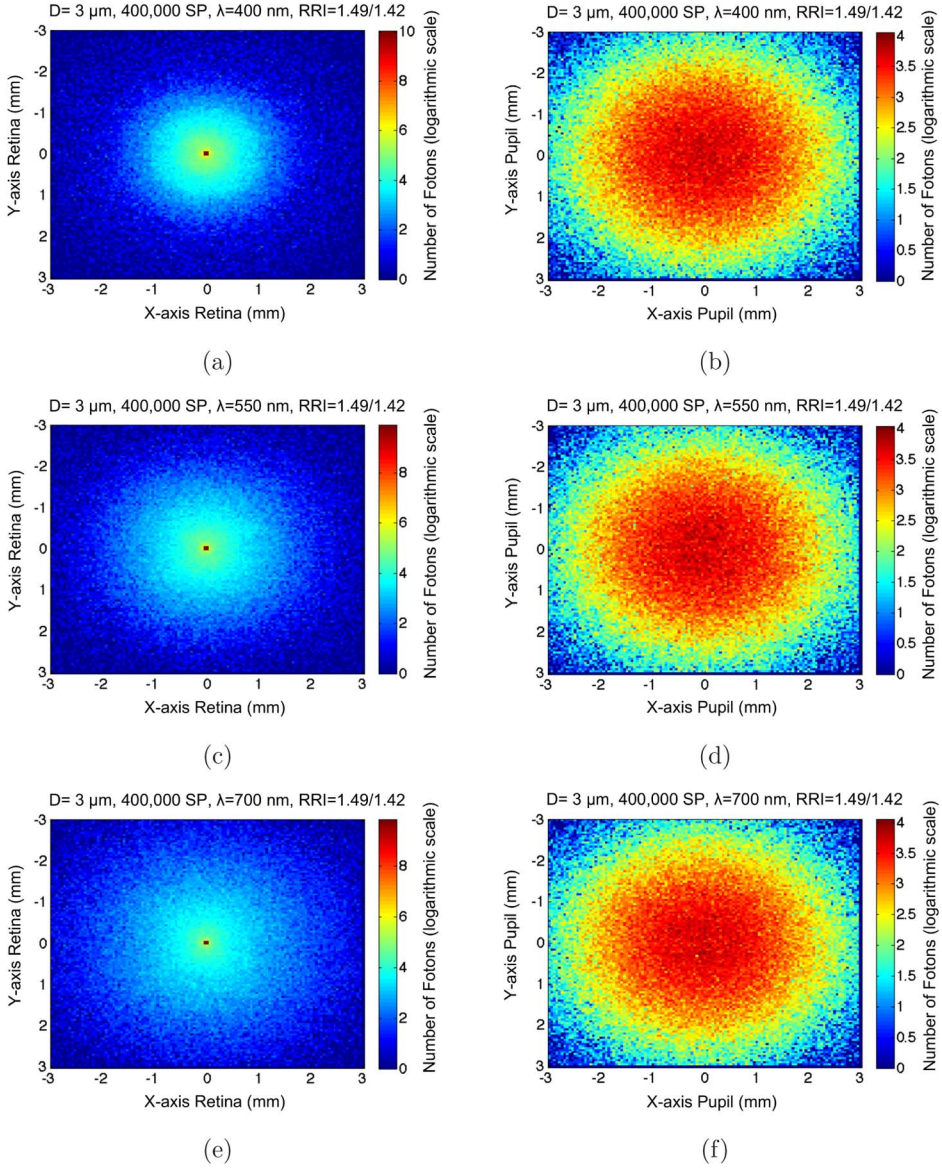

Fig. 2. Comparison of light intensity distribution between retina and pupil planes when wavelength is varying. SP, scattering particles.

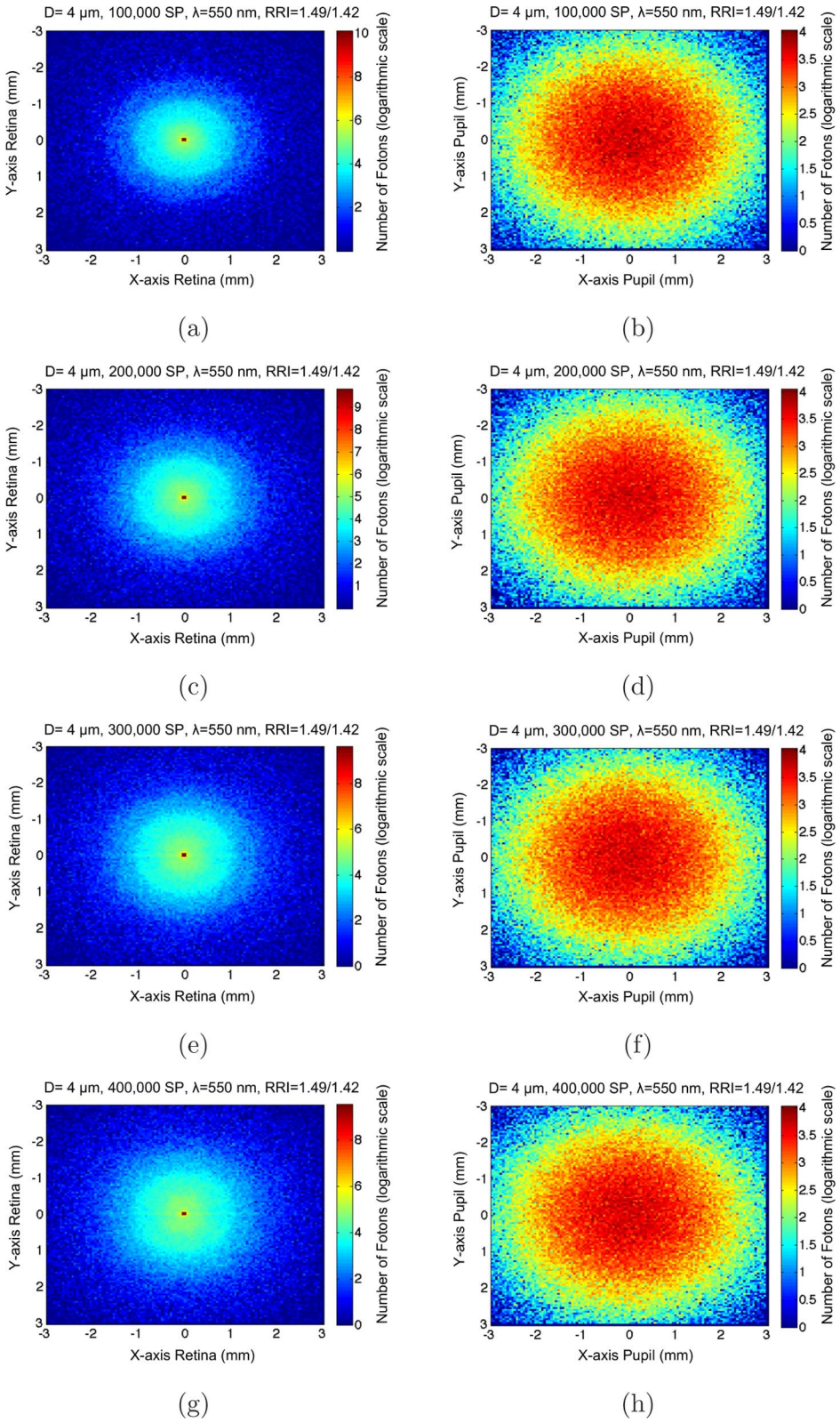

Fig. 3. Comparison of light intensity distribution between retina and pupil planes when density of particles is varying. SP, scattering particles.

4. DISCUSSION

From our results, we state that for the light pattern that is obtained on the plane of the exit pupil, there remain no traces that can help us to classify images that are formed in the plane of the retina, i.e., according to our computational model, it appears that there is no direct relationship between the image formation on the first and on the second pass when we measure the effect of the light scattering on both planes. The information obtained in the first pass indicates that particle size, wavelength, and the number of particles are factors that affect

the PSF. On the second pass, however, the effects of these factors are not appreciated so easily. Then, an analysis of the image formed in the exit pupil after the incident light has been reflected by the retina will not give us any important information about the degree of severity in an eye with cataracts and therefore, backward scattering is not useful as an index of the image degradation.

The Commission internationale d'Eclairage (CIE) has proposed several equations to determine the glare for a normal human eye [25]. Those equations represent how the light of a point source is distributed on the retina, i.e., they describe the PSF, including the effect of straylight, mainly caused by the interaction of light rays and the optical media of the human eye. Here, we use Eq. (26) found in "Report on disability glare" in the CIE Collection, 1999, to compare the PSF we obtained with our model with the PSF of the normal human eye.

$$\mathrm{PSF} = [L_{\mathrm{eq}}/E_{\mathrm{gl}}]_{\mathrm{gen}} = \frac{10}{\theta^3} + \left[\frac{5}{\theta^2} + 0.1 \times \frac{p}{\theta}\right] \times \left(1 + \left[\frac{A}{62.5}\right]^4\right) + 2.5 \times 10^{-3} \times p \tag{26}$$

Figure 4 shows the light intensity distributions of two cases using our model and the PSF function of a 65-year-old eye and a factor of pigmentation equal to 1, which was determined with the glare equation. The radial profiles of our simulations show that there is a stronger effect of scattering at the edges of the PSFs when there are cataracts, as is known to occur. To do the comparison, we selected the cases in which the size of the particles was 1 and 4 μm, with a total of 400,000 particles inside the lens. As we can notice even when the size of the particles is relatively small, there is more light distributed at the edge of the pattern than in the case of a normal human eye. An important point to observe is that the central peak in our simulations is narrower than that obtained with the glare equation. The reason for this is that in our simulation we have not considered the effect of diffraction.

As we have explained, after photons reach the retina, they are reflected back toward the exit pupil. To simulate this in our computational model, we considered the way light is distributed in the pupil plane according to the model of Marcos and Burns [23], which is based on two assumptions: the waveguide properties of the cones (Stiles–Crawford effect) and the interference of light at the pupil plane because each cone is considered to be a small coherent light source. The radial profiles shown in Fig. 5 compare the light intensity distribution in the exit pupil using Stiles–Crawford formula with three simulations of our model. The three simulated radial profiles are very similar to the form or shape of Stiles–Crawford formula, which confirms that our model is working in a proper manner. In the region very close to the optical axis, there are some variations in each of the simulated radial profiles, caused by the noise due to the random process of selection of the angle of reflection.

Figure 6 shows the radial profiles according to the light intensity distributions obtained in the exit pupil plane and the retina plane. In each subfigure, we compare four radial profiles, each of which corresponds to the effect of scattering related to the number of particles inside the lens. The images in the column to the left are the radial profiles of the retina plane and in the other column, the images correspond to the radial profiles of the pupil plane. These results confirm the reasoning with the images of the spots. In the retina plane, we can observe an increase in the intensities at the edges of the images, which depends on the number of scattering particles, and this variation is present in all cases of simulated particle sizes. In the subfigures, for the cases of the pupil plane, it can be seen that when we compare the four radial profiles, there is no significant difference between them and it is not possible to determine if an increase in the number of particles is generating any effect in the light distribution.

The results presented here suggest that the effect of retinal scattering with the model of Marcos and Burns [23] is more significant than the scattering effect induced by the particles, because retinal scattering dominates the second pass and the effect of the particles is hidden, which is noticeable in each

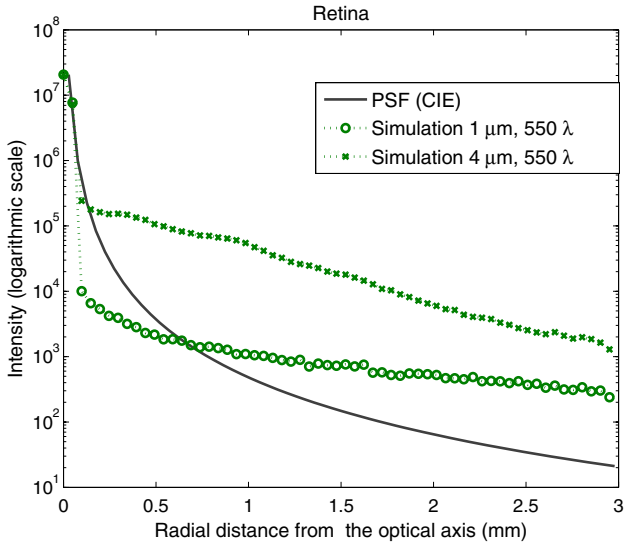

Fig. 4. Comparison between the PSF of the normal human eye using the CIE formula and the PSFs we obtained with our computational model.

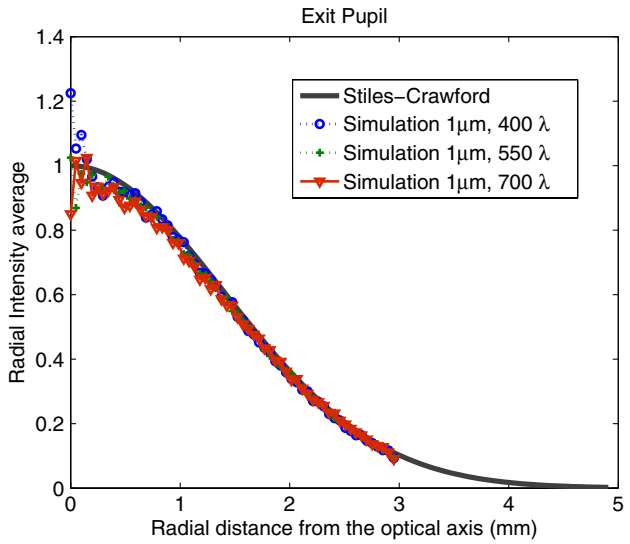

Fig. 5. Light distribution in the exit pupil using Stiles–Crawford formula with $\rho = 0.11$ according to Marcos and Burns [23] and the radial profiles of three cases using the computational model.

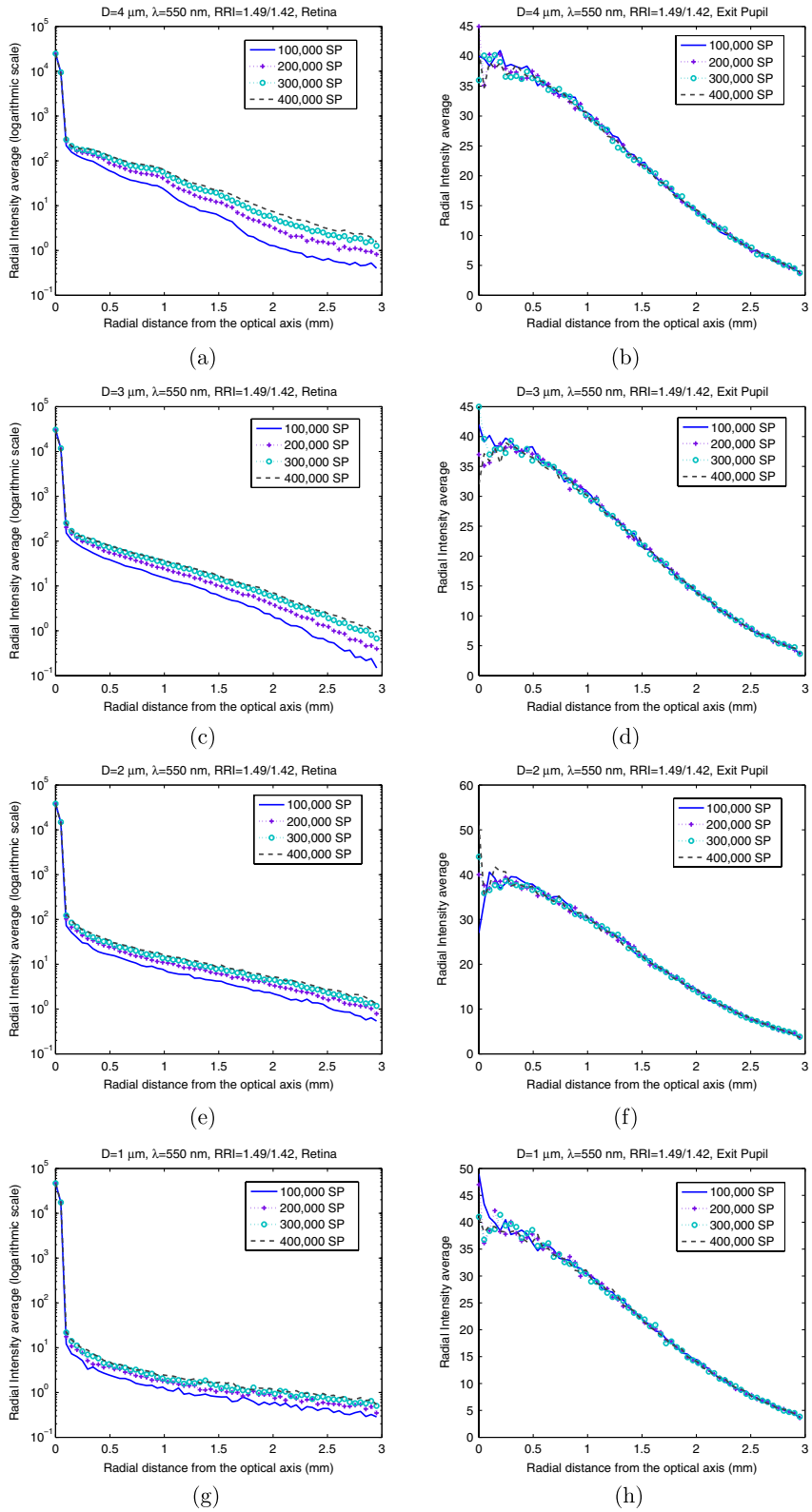

Fig. 6. Comparison of radial intensity profiles between retina and pupil planes when density of particles is variying. SP, scattering particles.

case we analyzed. We are continuing to work on the comparison of different models of retinal scattering to observe the effect these have on the total scattered light in the eye.

There are two experimental methods that measure retinal image quality in the human eye to predict cataract severity or forward scattering; both methods capture light that is reflected from the retina as it passes back through the lens. The method of Artal *et al.* [26] relates the light scattering at the periphery to light scattering in the center of the pattern, showing that what changes in the periphery is the intensity.

They relate variations of this intensity with the light scattering due to cataracts. On the other hand, the method of Donnelly *et al.* [27] is empirical. Donnelly *et al.* determine metrics of scattering pattern and show that their metrics are associated with reduced visual acuity, which is also measured. There is a need to quantify the light scattering as a function of position in the pupil to point out the measurements made in both methods. The method based on a double-pass system has the limitation of providing estimations of scattering for a small angle domain [28,29], where the level of scattering is minimal. In an eye affected by scatter, the wavefront obtained with a Hartmann–Shack wavefront sensor may fail to produce an overestimation of the image quality, due to limitation imposed by lens sampling [30]. It is noteworthy that the present article concerns areas of the PSF at larger distances than using the double-pass technique, and we are focusing our work to develop a model to quantify these measurements to make them more precise.

This work focuses on addressing the effect generated by scattering in the PSF and observing which are the characteristics that show an image affected by inhomogeneities such as those developed by the cataracts. The PSF in the pupil plane does not show explicit differences of the change in the scattering pattern when there are inhomogeneities in the lens; this result is confirmed when we obtain the radial profile of the PSF. To better relate the results obtained with our computational model with the results obtained with the methods of Artal *et al.* [26] and Donnelly *et al.* [27], we may simulate the PSF formed in the first step and define it within the area of registration done by both methods. According to our computational experiments, we can only establish that our results have some resemblance to those of the images obtained with the technique of Artal *et al.* [26].

We have to mention that our study on scattering derives its importance from the visual problem light scattering causes. The visual effect of light scattering is straylight; this effect is also called disability glare and is often the first complaint when cataract starts to develop. Determination of the level of ocular scattering is important for a better understanding of the visual performance of the patients [31,32].

According to our model, the size of the cataract particles is the most important parameter that affects the process of image formation. The size of particles is more important than the number of particles present. This happens because the total volume of the scatterers and the density vary more when we modify the size of the particles and maintain the number of elements than when we change the number and maintain the same particle size.

If inside the lens there are particles that vary in size between 1 and 4 μm, then the effect of scattering of light will be observed mainly at the borders of the PSF, generating a veil of light over the retina. This effect will be higher if a strong light source is presented in the field of view. Even though, according to Mie theory, the distribution function of the scattering angle becomes narrower as the size of the spherical particles increases, the effect of scattering can always be seen on the edges of the PSF, which increases the amount of light and generates more intense veiling light as particle size increases. This effect is because particles are distributed throughout the nucleus of the lens, and if the size of the particles increases, the probability that photons will collide with them will also increase, and therefore the light intensity increases in regions beyond the center of the PSF.

ACKNOWLEDGMENTS

I. Kelly-Pérez acknowledges CONACyT for a postdoctoral scholarship. We would like to express our gratitude to Dr. Thomas J. T. P. van den Berg for guidance on several points of this research.

REFERENCES

1. S. Dorairaj, V. Vatsala, J. Vijaya Kumar, R. Kesavai, D. Sucheethra, and S. Vidyasree, "Morphometric and histological study of human cataract lens," J. Anat. Soc. India **51**, 14–17 (2002).
2. F. Bettelheim and S. Ali, "Light scattering of normal human lens iii. Relationship between forward and back scatter of whole excised lenses," Exp. Eye Res. **41**, 1–9 (1985).
3. K. Gilliland, S. Johnsen, S. Metlapally, J. Costello, B. Ramamurthy, P. Krishna, and D. Balasubramanian, "Mie light scattering calculations for an Indian age-related nuclear cataract with a high density of multilamellar bodies," Mol. Vision **14**, 572–582 (2008).
4. T. Williamson, N. Strong, J. Sparrow, R. Aggarwal, and R. Harrad, "Contrast sensitivity and glare in cataract using the Pelli–Robson chart," Br. J. Ophtalmol. **76**, 719–722 (1992).
5. B. Friström and B. L. Lundth, "Colour contrast sensitivity in cataract and pseudophakia," Acta Ophthalmol. Scand. **78**, 506–511 (2000).
6. T. J. van den Berg, "Analysis of intraocular straylight, especially in relation to age," Optom. Vis. Sci. **72**, 52–59 (1995).
7. D. de Brouwere, "Corneal light scattering following excimer laser surgery," Ph.D. thesis (University of Crete, 2008).
8. T. J. van den Berg and H. Spekreijse, "Light scattering model for donor lenses as a function of depth," Vision Res. **39**, 1437–1445 (1999).
9. M. Costello, S. Johnsen, K. Gilliland, C. Freel, and W. Fowler, "Predicted light scattering from particles observed in human age-related nuclear cataracts using Mie scattering theory," Invest. Ophthalmol. Vis. Sci. **48**, 303–312 (2007).
10. R. Truscott, "Age-related nuclear cataract-oxidation is the key," Exp. Eye Res. **80**, 709–725 (2005).
11. K. Gilliland, C. Freel, C. Lane, W. Fowler, and M. Costello, "Multilamellar bodies as potential scattering particles in human age-related nuclear cataracts," Mol. Vis. **7**, 120–130 (2001).
12. D. A. Atchison and G. Smith, *Optics of the Human Eye* (Butterworth-Heinemann, 2000).
13. W. T. Welford, *Aberrations of Optical Systems* (IOP Publishing Ltd., 1986).
14. K. Gilliland, C. Freel, S. Johnsen, W. Fowler, and M. Costello, "Distribution, spherical structure and predicted Mie scattering of multilamellar bodies in human age-related nuclear cataracts," Exp. Eye Res. **79**, 563–576 (2004).
15. J. Illian, A. Penttinen, H. Stoyan, and D. Stoyan, *Statistical Analysis and Modelling of Spatial Point Patterns* (Wiley, 2008).
16. P. J. Diggle, *Statistical Analysis of Spatial Point Patterns* (A Hodder Arnold, 2003).
17. J. Antoch and G. Dohnal, eds., "Markov point process: 3D Voronoi tessellations generated by Strauss process," in *Robust 2000, Proceedings of the 11th Summer School JCMF* (JCMF, 2001), pp. 1–8.
18. H. C. van de Hulst, *Light Scattering by Small Particles* (Dover Publications Inc., 1981).
19. C. Bohren and D. Huffman, *Absorption and Scattering of Light by Small Particles* (Wiley, 1983).
20. V. E. Cachorro and L. L. Salcedo, "New improvements for Mie scattering calculations," J. Electromagn. Waves Appl. **5**, 913–926 (1991).
21. H. Du, "Mie-scattering calculation," Appl. Opt. **43**, 1951–1956 (2004).
22. S. Marcos, S. A. Burns, and J. C. He, "Model for cone directionality reflectometric measurements based on scattering," J. Opt. Soc. Am. A **15**, 2012–2022 (1998).

23. S. Marcos and S. A. Burns, "Cone spacing and waveguide properties from cone directionality measurements," J. Opt. Soc. Am. A **16**, 995–1004 (1999).
24. C. Bohren and E. Clothiaux, *Fundamentals of Atmospheric Radiation* (Wiley-VCH Verlag, 2006).
25. T. J. van den Berg, L. Franssen, and J. Coppens, "Ocular media clarity and straylight," in *Encyclopedia of the Eye*, D. A. Dartt, J. C. Besharse, and R. Dana, eds. (Academic, 2010), Vol. **3**, pp. 173–183.
26. P. Artal, A. Benito, G. M. Pérez, E. Alcón, A. de Casas, J. Pujol, and J. M. Marín, "An objective scatter index based on double-pass retinal images of a point source to classify cataracts," PLoS One **6**, e16823 (2011).
27. W. J. Donnelly III, K. Pesudovs, J. D. Marsack, E. J. Sarver, and R. A. Applegate, "Quantifying scatter in Shack–Hartmann images to evaluate nuclear cataract," J. Refract. Surg. **20**, 515–522 (2004).
28. N. López-Gil and P. Artal, "Comparison of double-pass estimates of the retinal-image quality obtained with green and near-infrared light," J. Opt. Soc. Am. A **14**, 961–971 (1997).
29. P. Rodríguez and R. Navarro, "Double-pass versus aberrometric modulation transfer function in green light," J. Biomed. Opt. **12**, 044018 (2007).
30. F. Díaz-Douton, A. Benito, J. Pujol, M. Arjona, J. L. Güell, and P. Artal, "Comparison of the retinal image quality with a Hartmann–Shack wavefront sensor and a double-pass instrument," Investig. Ophthalmol. Vis. Sci. **47**, 1710–1716 (2006).
31. P. W. de Waard, J. K. IJspeert, T. J. van den Berg, and P. T. de Jong, "Intraocular light scattering in age-related cataracts," Invest. Ophthalmol. Vis. Sci. **33**, 618–625 (1992).
32. T. J. van den Berg, L. Frassen, B. Krujit, and J. E. Coopens, "History of ocular straylight measurement," Invest. Ophthalmol. Vis. Sci. **23**, 6–20 (2013).